



Cerium metal-organic framework composited with polyaniline on carbon cloth for high-sensitively electrochemical sensing of carbendazim

Rui Zhou^a, Ling-Zhi Liu^a, Yue-Hong Pang^{a,b}, Xiao-Fang Shen^{a,b,*}

^a State Key Laboratory of Food Science and Resources, School of Food Science and Technology, Collaborative Innovation Center of Food Safety and Quality Control in Jiangsu Province, Jiangnan University, Wuxi 214122, China

^b International Joint Laboratory on Food Safety, Jiangnan University, Wuxi 214122, China

ARTICLE INFO

Keywords:
Ce-MOF
Polyaniline
Carbendazim
Carbon cloth
Electrochemical sensor

ABSTRACT

Carbendazim (CBZ) has generated significant attention due to potential harm to human health, thus developing a simple and economy-friendly approach for determining CBZ is vital. Herein, Cerium metal-organic framework (Ce-MOF) and polyaniline (PANI) were composited under mild condition and modified on carbon cloth (CC) to fabricate an electrochemical sensor based on Ce-MOF@PANI/CC for fast and sensitive determination of CBZ. Rod-shaped Ce-MOF facilitated the dispersion of PANI, while the doping of PANI improved conductivity of Ce-MOF to amplify detection signal. Moreover, the modification of Ce-MOF@PANI on CC increased the electrochemical active area of CC by 2.78 times. Under optimized conditions, the method demonstrated a linear range of 0.1–80 μM and a detection limit of 12.6 nM. Additionally, the response value of the sensor to CBZ still maintained 94.32% of the initial value after 15 days. It also had good reproducibility and anti-interference. The sensor was utilized for detecting CBZ in fruit (apple, pear), vegetables (tomato, cucumber), and water (lake, tap water) with recovery of 92.31%–105.47% consistent with those of high-performance liquid chromatography.

1. Introduction

Carbendazim (CBZ) is extensively utilized for the prevention of various pathogens in fruit and vegetables [1,2]. The residue of CBZ easily posed serious effects on humans because of the stable structure of the benzimidazole ring [3]. It could disrupt the endocrine system and induce cancer [4,5]. CBZ was detected with a maximum reaching 1396 ng/L in watercourse and was also discovered in fruit and vegetables [6–8]. In International Codex Alimentarius Commission, maximum residue limits for CBZ have been regulated with the range of 0.05–20 mg/kg in crops [9]. Therefore, the accurate determination of CBZ is extremely significant to both environmental preservation and human health.

Many analytical methods, such as liquid chromatography-mass spectrometry (LC-MS) [10], high-performance liquid chromatography (HPLC) [2], capillary electrophoresis [11], and immunoassay [12] have been applied to the determination of CBZ. These methods need time-consuming pre-treatments and high cost [13]. Electrochemical method, known for its easy operation, low cost, and rapid response, has been extensively employed in the analysis of heavy metal ions, food

additives, bioactive molecules, and environmental pollutants [14–17]. It has potential to be utilized for the rapid detection of CBZ. Electrode substrates and electrode modification materials are key factors to enhance the sensitivity of this method. Previous electrode substrate detecting CBZ focused on traditional glassy carbon electrode (GCE). Flexible electrode substrates have higher conductivity compared with GCE and have generated increasing research interest in electrochemical sensing [18]. Carbon cloth (CC), as a flexible electrode easily prepared, possessed commendable conductivity along with substantial specific surface area. CC was modified by adding functional materials to further improve sensor sensitivity. Modification materials are also a key to enhance the sensitivity of electrochemical determination.

Metal-organic frameworks (MOFs), a class of emerging porous nanomaterials, have garnered considerable attention in the field of electrochemistry [19]. Singh et al. [20] conducted the synthesis of Cu-MOF to enable the sensitive detection of Hg^{2+} in canned tuna fish and tap water. Mahmoudi et al. [21] fabricated an electrochemical biosensor based on Ce/Uio-66@MWCNTs for detecting organophosphate pesticide in cabbage and spinach. Cerium (Ce) stands out as a highly abundant rare earth element and has been applied to synthesize various

* Corresponding author at: State Key Laboratory of Food Science and Resources, School of Food Science and Technology, Collaborative Innovation Center of Food Safety and Quality Control in Jiangsu Province, Jiangnan University, Wuxi 214122, China.

E-mail address: xfshen@jiangnan.edu.cn (X.-F. Shen).

<https://doi.org/10.1016/j.microc.2023.109862>

Received 15 November 2023; Received in revised form 20 December 2023; Accepted 22 December 2023

Available online 23 December 2023

0026-265X/© 2023 Elsevier B.V. All rights reserved.

functional nanomaterials [22,23]. Notably, Ce-MOF exhibited milder synthesis condition relative to other MOFs [24]. The higher coordination number and variable valence-state of Ce make Ce-MOF have excellent redox ability. Moreover, Ce-MOF had the potential to promote the enrichment of analytes through hydrogen bonding interaction and π - π stacking [25]. To further improve electron transfer rates enhancing the electrochemical performance of Ce-MOF, it was worth utilizing a functional material with easy synthesis and superior performance for fabricating composite. Tu et al. [26] fabricated reduced graphene oxide-encapsulated Ce-MOF to determine dichlorophen. Wang et al. [27] synthesized 2D carbon nanotube@Ce-MOF nanosheet hybrid materials for the effective detection of nitrites. Chen et al. [28] devised a sensor utilizing Ce-MOF/Ti₃C₂T_x MXene composite for electrochemical detection of L-Tryptophan. Polyaniline (PANI), a conductive polymer, holds great potential in various applications owing to its advantageous attributes including high conductivity, low cost, and remarkable redox properties. Furthermore, PANI can be conveniently synthesized at room temperature, distinguishing it from alternative functional materials like noble metal nanoparticles and carbon nanotubes [29–31]. PANI with the extended π conjugated system was doped to Ce-MOF and conducive to amplifying detection signal. It could be expected that the materials formed by the composite of Ce-MOF and PANI could take on better electrochemical properties.

Herein, Ce-MOF and PANI were synthesized by mild and simple hydrothermal method and chemical oxidative polymerization method individually. The raw materials required for their production were readily accessible, which was economy-friendly. Ce-MOF@PANI composite was fabricated using a straightforward ultrasonic method and modified on CC to prepare Ce-MOF@PANI/CC electrode for sensitive electrochemical sensing of CBZ via differential pulse voltammetry (DPV). The methodology evaluation and catalytic mechanism of determining CBZ were further explored by cyclic voltammetry (CV) and DPV after analyzing the characterization and electrochemical properties of Ce-MOF@PANI. Additionally, the developed sensor demonstrated successful application in practical analysis (fruit, vegetables, and water).

2. Experiment

2.1. Fabrication of Ce-MOF@PANI

2.1.1. Synthesis of PANI and Ce-MOF

PANI was obtained using a chemical oxidation polymerization procedure [29]. Typically, aniline (0.25 M) was put into a solution of dilute hydrochloric acid (20 mL) while being continuously stirred for 30 min. Subsequently, 0.2 M ammonium persulfate in 30 mL dilute hydrochloric acid was gradually added to the solution obtained earlier. Following 12 h of constant stirring, the resultant mixture yielded green precipitate, which was centrifuged at 10000 rpm for 8 min. The precipitate was then subjected to a washing process using ethanol and water. Ultimately, the precipitate was dried for 12 h at 60°C to obtain PANI.

Ce-MOF was prepared using a hydrothermal approach with slight modifications, following the procedure described in the literature [32]. Trimesic acid (0.22 M) and Ce(NO₃)₃·6H₂O (0.22 M) were gradually added to a mixture of water/ethanol (v/v = 3:1, 45 mL) under stirring at 60°C for 1 h. A significant quantity of white precipitate was obtained through centrifugation at a speed of 10000 rpm for 5 min, with the purpose of isolating the precipitate of Ce-MOF. Subsequently, the precipitate underwent washing with ethanol and water to eliminate residual reactants, followed by drying for 12 h at 60°C.

2.1.2. Synthesis of Ce-MOF@PANI

A straightforward method was conducted to synthesize Ce-MOF@PANI. Ce-MOF (20 mg) and PANI (10 mg) were put into 10 mL water/ethanol mixture. The resulting mixture was subjected to ultrasonic mixing for 1 h, which was then centrifuged at 10000 rpm for 5 min to obtain Ce-MOF@PANI precipitate. The precipitate underwent

washing with ethanol and water and was subsequently dried for 12 h at 60°C.

2.2. Preparation of Ce-MOF@PANI/CC

Commercial CC was cut into rectangular pieces (1.5 × 1.0 cm²). CC was ultrasonically cleaned in dilute nitric acid for 30 min before modification. Then ultrasonically clean for 5 min in acetone, anhydrous ethanol, and water, respectively. CC was then dried at 60°C in preparation for use. Subsequently, 18 μ L Ce-MOF@PANI (1 mg/mL) water/ethanol solution was dripped on the center of CC and dried at 60°C. Ce-MOF@PANI/CC was fabricated for use.

2.3. Electrochemical experiments

CV and electrochemical impedance spectroscopy (EIS) were carried out to evaluate the electrochemical characteristics of the electrodes in 1.0 mM [Fe(CN)₆]^{3-/4-}. CV had a potential ranging from -0.20 V to 0.60 V. The EIS measurements were performed with frequency range of 0.01 Hz to 100000 Hz, while the amplitude was 5 mV. CBZ was determined via DPV scanning with the range of 0.5–0.9 V by using a 0.05 V amplitude and a 0.05 s pulse width. The electrolyte used for the electrochemical experiments was phosphate buffer solution (PBS, 0.1 M) with pH 7.0.

3. Results and discussion

3.1. Construction of Ce-MOF@PANI/CC electrochemical sensor for detecting CBZ

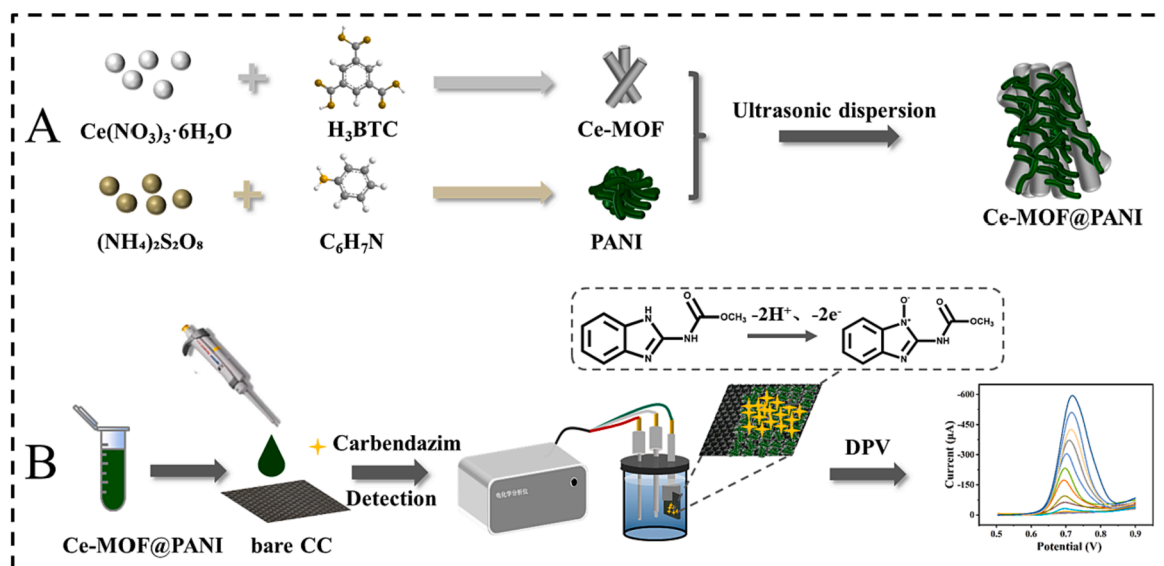
The fabrication route of Ce-MOF@PANI was illustrated in Scheme 1A and the electrochemical sensor based on Ce-MOF@PANI/CC for detecting CBZ was shown in Scheme 1B. CBZ has the benzimidazole ring structure with molecular diameter of about 1.1 nm (Fig. S1C). Ce was chosen as the central metal to improve the redox ability of Ce-MOF due to the variable valence-state [24]. Owing to the limited electron transfer rate of Ce-MOF, PANI, a conductive polymer with the extended π conjugated system, was compounded to Ce-MOF to further enhance the conductivity of Ce-MOF amplifying detection signal. Ce-MOF@PANI with a pore size of approximately 3.67 nm (Fig. S1B) was potentially suited for promoting the accumulation of CBZ on the electrode surface through pore-size matching effect and π - π stacking. In summary, the composite of Ce-MOF and PANI was modified on CC to prepare electrochemical sensing platform based on Ce-MOF@PANI/CC to detect CBZ in fruit, vegetables, and water.

3.2. Characterization of Ce-MOF@PANI

3.2.1. Morphology characterization

Scanning electron microscope (SEM) was conducted to explore the morphology of PANI, Ce-MOF, and Ce-MOF@PANI. As depicted in Fig. S2A, Ce-MOF was typically rod-shaped like natural wheatears with lengths from 2 to 5 μ m [32]. PANI exhibited nanofibers structure consistent with findings documented in prior literature (Fig. S2B) [33]. Fig. 1C showed that the surface of rod-shaped Ce-MOF was decorated with nanofibers and indicated the successful synthesis of Ce-MOF@PANI. The morphological analysis of the composite revealed that the incorporation of PANI did not induce any alterations in the morphology of Ce-MOF, while Ce-MOF contributed to a better dispersion of PANI and further increased active sites of the composite.

The surface morphology of the pretreated CC and Ce-MOF@PANI/CC were further characterized by SEM. As shown in Fig. 1A, CC was made up of interlaced carbon fibers without impurities. As Fig. 1B displayed, CC was modified with Ce-MOF@PANI whose morphology was further illustrated in Fig. 1C, revealing the successful fabrication of Ce-MOF@PANI/CC electrode.



Scheme 1. (A) Construction of Ce-MOF@PANI/CC and (B) electrochemical approach for detecting CBZ.

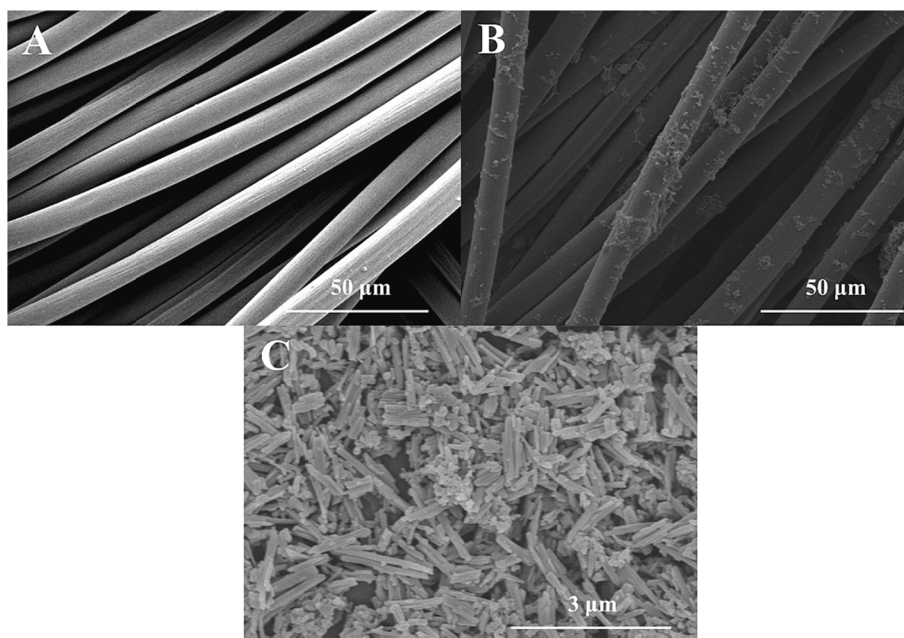


Fig. 1. SEM images of (A) bare CC, (B) Ce-MOF@PANI/CC, and (C) Ce-MOF@PANI.

3.2.2. Functional groups and chemical bonds

The utilization of Fourier transform infrared spectra (FT-IR) was carried out to investigate the functional groups and chemical bonds of PANI, Ce-MOF, and Ce-MOF@PANI. As the FT-IR spectrum illustrated (Fig. S3A), the characteristic peak of Ce-O bond appeared at 530 cm^{-1} [34]. The peak of 3400 cm^{-1} was regarded as the O-H stretching vibration originating from the water molecule, demonstrating Ce-MOF was prepared successfully [25]. Furthermore, the composite exhibited characteristic peaks at $1610\text{--}1560\text{ cm}^{-1}$ and $1435\text{--}1370\text{ cm}^{-1}$, identified as the asymmetric stretching vibrations and the stretching vibrations belonged to the carboxylate ions of the ligand, which was consistent with absorption spectrum of Ce-MOF [35]. The strong peaks of 1570 cm^{-1} and 1482 cm^{-1} were regarded as the C=N and C=C stretching vibrations, which were associated with the quinone and benzene rings present in PANI [36]. Moreover, the presence of the benzenoid unit could be inferred from the identification of characteristic peaks of C-N

stretching vibration located at 1306 cm^{-1} . Additionally, the characteristic peak of 1240 cm^{-1} and 1145 cm^{-1} was indicative of the stretching mode of the C-H from benzenoid and quinoid rings [37]. The FT-IR spectrum of the Ce-MOF@PANI composite also demonstrated the characteristic peaks of PANI (Fig. S3A). Combined with the above results, Ce-MOF@PANI was successfully compounded.

3.2.3. Crystalline structures

The crystalline structures of PANI, Ce-MOF, and Ce-MOF@PANI were characterized via X-ray diffraction (XRD). As Fig. S3B illustrated, the diffraction peak observed at 25.10° was consistent with the (200) crystal plane in PANI, originating from the periodicity which was parallel to the polymer chains [29]. The main diffraction peaks sharp and clear appeared at 10.15° , 13.28° , and 17.32° demonstrating the excellent crystallinity of Ce-MOF in accord with the published literature [32]. Moreover, the characteristic diffraction peaks of the composite showed

the Ce-MOF characteristic and expressed that the doping of PANI had not changed the crystalline structure of Ce-MOF.

3.2.4. Chemical states and elemental compositions

The utilization of X-ray photoelectron spectroscopy (XPS) was employed to investigate the chemical states and elemental compositions of Ce-MOF@PANI. As shown in Fig. S4, the composite had elements C, Ce, O, and N, conforming successful synthesis of Ce-MOF@PANI. The three deconvoluted characteristic peaks of 288.7 eV (O-C-O), 286.7 eV (C-N), and 284.8 eV (C-C) were observed in high resolution C 1s spectra (Fig. 2A) [38]. Fig. 2B indicated that the XPS spectra of Ce 3d contained two multiplets, associated with 3d_{5/2} and 3d_{3/2} core holes from the spin-orbit split [39]. The presence of two peaks at 904.1 eV and 885.4 eV in the XPS spectra was attributed to the characterization of Ce³⁺ in the composite. Additionally, the four peaks at 882.3 eV, 887.0 eV, 900.6 eV, and 906.8 eV were found to be associated with Ce⁴⁺. These findings suggested that Ce in Ce-MOF@PANI exhibited a mixed valence-state [24]. The XPS spectra of O 1s exhibited peaks of 531.6 eV (Ce-O) and 532.2 eV (C=O), as shown in Fig. 2C [37]. The peaks of N 1s of XPS spectra were centered respectively at 399.2 eV and 402.3 eV matching with undoped imine units -N= and -NH- in Fig. 2D [40].

3.2.5. Specific surface area

The measurement of specific surface area for Ce-MOF and Ce-MOF@PANI was conducted using Nitrogen adsorption-desorption isotherms. The isotherms of Ce-MOF and Ce-MOF@PANI were an IV-type curve typically, as illustrated in Fig. S1A, B [40]. The specific surface area for Ce-MOF was 33.35 m²/g and Ce-MOF@PANI was 44.11 m²/g, demonstrating the specific surface area of Ce-MOF was slightly improved due to the doping of PANI.

3.3. Electrochemical characterizations of Ce-MOF@PANI/CC

The electrochemical properties of bare CC and other different electrodes containing Ce-MOF/CC, PANI/CC, and Ce-MOF@PANI/CC were

investigated by CV in 1.0 mM [Fe(CN)₆]^{3-/4-} solution. Ce-MOF/CC exhibited a higher peak current (312.1 μA) compared to bare CC (261.8 μA) since Ce-MOF had good redox ability, as shown in Fig. 3A [35]. CC modified with PANI showed a further increase of current (570.4 μA), which was attributed to the ability of partial oxidized phase states of PANI to enhance the electrical conductivity [29]. Notably, Ce-MOF@PANI/CC demonstrated the highest response current (784.1 μA), implying the synergistic effect between Ce-MOF and PANI could improve charge transfer capability.

EIS can characterize the resistive properties, and further compare the difference in conductivity between different electrodes. The diameter of the semicircle of Nyquist plots exhibits a positive correlation with the charge transfer resistance (R_{ct}), standing for the electron transfer efficiency [41]. The R_{ct} of different electrodes decreased due to the drop coating of Ce-MOF, PANI, and Ce-MOF@PANI compared to bare CC, as illustrated in Fig. 3B. In particular, the Ce-MOF@PANI/CC had a minimum R_{ct}, demonstrating a terrific electron transfer process.

The electrochemical active surface area of different electrodes, including bare CC, Ce-MOF/CC, PANI/CC, and Ce-MOF@PANI/CC were investigated by analyzing the peak current at various scan (0.02–0.2 V/s) in 1.0 mM [Fe(CN)₆]^{3-/4-} solution (Fig. S5). With the increasing scan rate, the I_{pa} and I_{pc} of Fe²⁺/Fe³⁺ redox couple on bare CC, Ce-MOF/CC, PANI/CC, and Ce-MOF@PANI/CC gradually expanded. The square root of the scan rate (v^{1/2}) was positively correlated to the peak currents of I_{pa} and I_{pc}, implying the diffusion condition governed the electrochemical reaction of Fe²⁺/Fe³⁺ [27]. Particularly, the slope of I_{pa} and I_{pc} to v^{1/2} of Ce-MOF@PANI/CC was the largest based on the fitting equation (Fig. S5H). The calculation of the effective active surface area of different modified electrodes was carried out utilizing the Randles-Sevcik equation, which was shown in Eq. (1) [42]:

$$I_p = 2.69 \times 10^5 ACD^{1/2} n^{2/3} \nu^{1/2} \quad (1)$$

It was calculated that the electrochemical active surface area for bare CC was 2.71 cm², Ce-MOF/CC was 2.98 cm², PANI/CC was 7.11 cm², and Ce-MOF@PANI/CC was 10.24 cm². Ce-MOF/CC exhibited a slight

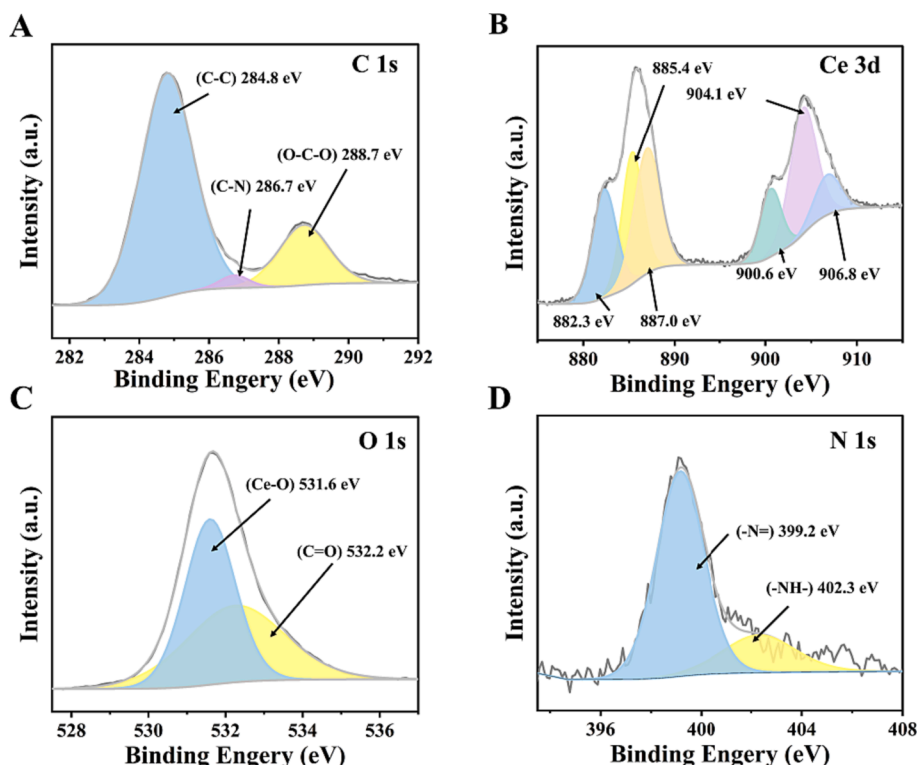


Fig. 2. XPS survey spectra Ce-MOF@PANI of (A) C 1s, (B) Ce 3d, (C) O 1s, and (D) N 1s.

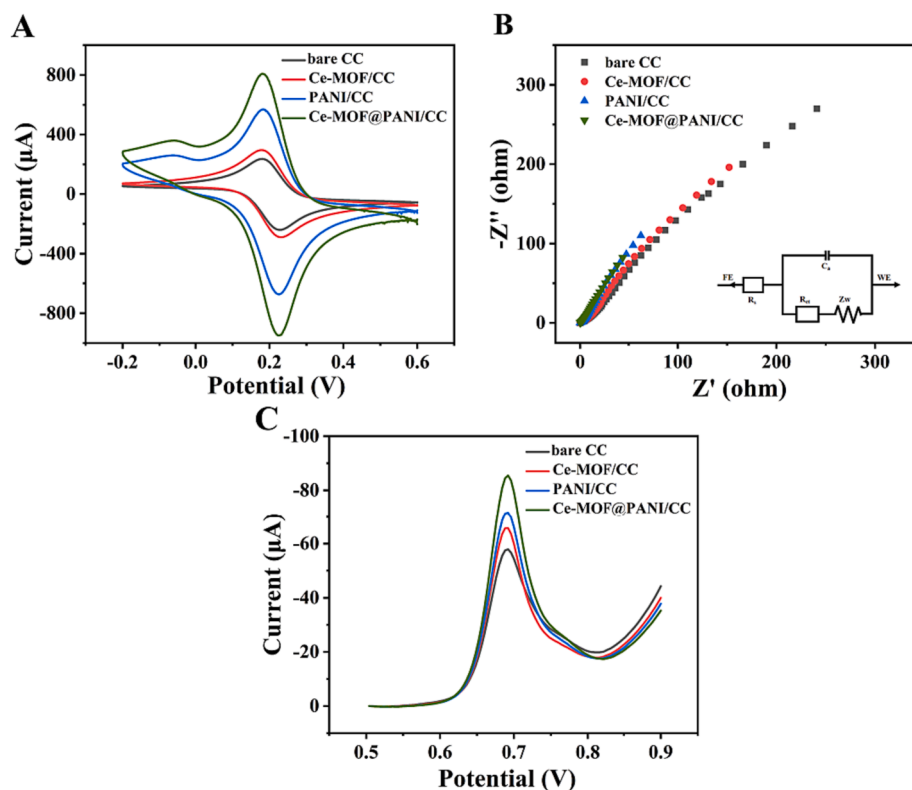


Fig. 3. (A) CV (scan rate: 0.04 V/s) and (B) EIS curves of bare CC, Ce-MOF/CC, PANI/CC, and Ce-MOF@PANI/CC in 1.0 mM $[\text{Fe}(\text{CN})_6]^{3-/4-}$ solution; (C) DPV responses to CBZ on bare CC, Ce-MOF/CC, PANI/CC, and Ce-MOF@PANI/CC electrodes.

increase in electrochemical active surface area when compared to bare CC. Moreover, the modification of PANI further increased the electroactive area by 2.78 times, proving that PANI and Ce-MOF synergistically enhanced conductivity of the composite-modified electrodes and facilitated electron transfer.

3.4. Electrochemical response to CBZ on different electrodes

The electrochemical response to CBZ on bare CC, Ce-MOF/CC, PANI/CC, and Ce-MOF@PANI/CC electrodes were displayed in Fig. 3C. The electrochemical response of bare CC to CBZ was the smallest (46.34 μA). With the modification of Ce-MOF, the response for CBZ increased to 55.34 μA , attributed to the variable valence-state of Ce possessing good redox ability [39]. Moreover, the doping of PANI with high electrical conductivity further promoted efficient electrochemical oxidation of CBZ to amplify detection signal and made the Ce-MOF@PANI/CC electrode have the largest current response (75.70 μA).

The possible interaction between CBZ and Ce-MOF@PANI was investigated by exploring the fluorescence response of CBZ, Ce-MOF@PANI, and Ce-MOF@PANI + CBZ. As seen from Fig. S6A, the fluorescence intensity of Ce-MOF@PANI slightly decreased after adding CBZ, indicating π - π stacking existed between CBZ and Ce-MOF@PANI resulting in fluorescence quenching [43]. The functional groups of CBZ, Ce-MOF@PANI and Ce-MOF@PANI + CBZ were explored employing FT-IR (Fig. S6B). The FT-IR spectrum analysis revealed that both three exhibited a cluster of peaks within the 1300 to 1500 cm^{-1} range, indicative of the presence of the aromatic compounds. The FT-IR spectrum of Ce-MOF@PANI + CBZ demonstrated that no new compound was formed since the addition of CBZ did not yield any significant emergence of novel functional groups [43]. The UV-vis absorption spectra of CBZ and Ce-MOF@PANI + CBZ were identical (Fig. S6C), which also suggested the absence of any new compound formation between Ce-MOF@PANI and CBZ [5]. These aforementioned results above indicated the presence of the benzene ring from Ce-MOF@PANI and

CBZ, which suggested that Ce-MOF@PANI could enrich more CBZ via π - π stacking.

3.5. Study on electrochemical reaction mechanism of CBZ

The CV response of Ce-MOF@PANI/CC electrode to CBZ was investigated by varying the scan rate (0.04–0.2 V/s). The peak current response to CBZ progressively enlarged as the scan rate increased (Fig. S7A). The correlation between the scan rate and the peak current was found to be linear (Fig. S7A), with the equation $I = -89.651v + 0.412$ ($R^2 = 0.9889$). The linear correlation suggested that the adsorption process governed the electrochemical reaction process of CBZ at the Ce-MOF@PANI/CC electrode surface. The linear regression equation, $E_{pa} = 0.0115\ln v + 0.762$ ($R^2 = 0.9868$), was derived to demonstrate a good linear correlation between potential and logarithms of scan rates in Fig. S7B [44]. By employing the Butler-Volmer equation, which was shown in Eq. (2) [45]:

$$E_{pa} = E^0 - (RT/anF)\ln(RTks/anF) + (RT/2anF)\ln v \quad (2)$$

n representing the electron transfer number was calculated by taking the slope of the E_{pa} - $\ln v$ plot, which was equal to $RT/2anF$, where α stands for the electron transfer coefficient, F , R , and T are the constants, and E_{pa} represents the potential [45]. Hence, it was calculated that there were roughly 2 electrons transferred of CBZ on the Ce-MOF@PANI/CC electrode surface. Additionally, the potential of CBZ at different pH was studied (Fig. S8). A strong linear correlation was observed between the peak potential of CBZ and pH, with the linear equation $E_{pa} = -0.0640\text{pH} + 1.156$ ($R^2 = 0.9871$), indicating the involvement of protons in the oxidation process, as depicted in Fig. S8B [45]. The measured slope of -64.0 mV/pH closely approximated the theoretical slope of -59.1 mV/pH, exposing that the numbers of protons and electrons transferred were equal in the oxidation of CBZ [46]. Based on the aforementioned results, it could be deduced that the electrochemical

oxidation process of CBZ on the Ce-MOF@PANI/CC electrode involved the transfer of two protons and two electrons (Fig. S9) [47].

3.6. Optimal conditions for electrochemical detection

The pH of PBS significantly influences the electrochemical oxidation of CBZ. The optimization of pH ranging from 4.0 to 9.0 was investigated using DPV, as displayed in Fig. S8. The peak current gradually decreased from 7.0 to 9.0, possibly ascribed to CBZ getting solidified in acidic condition and degraded under alkaline environment, after reaching the highest peak current of CBZ at pH 7.0 [48]. Consequently, pH 7.0 was deemed to be the most appropriate pH in the subsequent experiments.

The correlation between the peak current response to CBZ and different adsorption time was investigated via DPV. The peak current of CBZ gradually improved as the adsorption time increased from 0 to 180 s (Fig. S10), attributed to the enrichment of CBZ on Ce-MOF@PANI/CC surface. Afterwards, as a result of the saturation of CBZ adsorption, the peak current brought about a slight change with the prolongation of adsorption time from 180 to 240 s on the electrode surface (Fig. S10). Therefore, the adsorption time of 180 s was deemed to be the most favorable time for adsorption.

3.7. Method validation

3.7.1. Electrochemical detection of CBZ

The electrochemical detection performance of CBZ based on Ce-MOF@PANI/CC sensor was investigated under optimal conditions in different concentrations with a range of 0.1–80 μM . DPV was employed to analyze the correlation between the peak current and different CBZ concentrations. Fig. 4A illustrated the impact of varying CBZ concentrations on the peak current. Different CBZ concentrations and the peak current exhibited a positive correlation. As shown in Fig. 4B, this correlation was represented by the linear equation $I = -7.205C + 0.604$ ($R^2 = 0.9973$). Through analytical calculations, the low limit of detection (LOD) was calculated to be up to 12.6 nM ($S/N = 3$) [49].

The comparison between the performance of the Ce-MOF@PANI/CC and other electrodes were presented in Table 1. Ce-MOF@PANI/CC had a lower detection limit and a broader linear range to detect CBZ. In addition, the remarkable electrochemical characteristics of Ce-MOF@PANI were ascribed to the exceptional redox ability and conductivity from Ce-MOF and PANI. The pore size of synthesized Ce-MOF@PANI surpassed the dimensions of CBZ (Fig. S1), thereby facilitating the effective enrichment of CBZ. Ce-MOF@PANI/CC was easy to fabricate and their excellent electrochemical active surface area obtained from Ce-MOF@PANI made it suitable for detecting CBZ.

3.7.2. Reproducibility, stability, and anti-interference studies

8 electrodes were fabricated to measure CBZ to evaluate the

Table 1

Comparison of the Ce-MOF@PANI/CC electrode for the detection of CBZ with some other electrodes.

Electrode	Linear range (μM)	LOD (nM)	References
NP-Cu/RGO/GCE	0.5–30	90	[50]
La-Nd ₂ O ₃ /CPE	0.08–50	27	[51]
MBC@CTS/GCE	0.1–20	20	[52]
SiO ₂ /MWCNT/GCE	0.2–4	56	[53]
MWCNT/GCE	0.256–3.11	54.9	[54]
CNTs-MAS _{4,8} /GCE	0.1–2	40	[55]
Ce-MOF@PANI/CC	0.1–80	12.6	This work

reproducibility. Fig. S11A demonstrated that 8 electrodes displayed a comparable peak current, accompanied by a relative standard deviation (RSD) of 3.22%, demonstrating Ce-MOF@PANI/CC had excellent reproducibility. Furthermore, the long-term storage stability of Ce-MOF@PANI/CC was investigated by monitoring the peak current response to CBZ over 15 days. As observed in Fig. S11B, the peak current response to CBZ at Ce-MOF@PANI/CC electrode surface gradually decreased and maintained approximately 94.32% of its original value after 15 days, indicating excellent long-term storage stability of electrode. Signal variation of the peak current response to CBZ was monitored in the presence of 10-fold concentration of K⁺, Na⁺, Mg²⁺, Al³⁺, Ca²⁺, Cl⁻, SO₄²⁻, NO₃⁻, glucose, urea, ascorbic acid, glyphosate, trichlorfon, dimethoate, imidacloprid, dinotefuran, and thiamethoxam in order to verify the selectivity of Ce-MOF@PANI/CC sensor (Fig. S12). The aforementioned interferences had no impact on the detection of CBZ, as evidenced by the RSD of 3.06%. These results suggested that the sensor exhibited a strong capability to resist interferences.

3.8. Analytical application

The fabricated sensor was conducted to measure CBZ in fruit and vegetables samples (apple, pear, tomato, and cucumber) and water samples (lake, tap water) to investigate the effectiveness of the developed sensor. As Table 2 displayed, the observed recovery ranged from 92.31% to 105.47%, and the RSDs were controlled within 7.15% in the actual samples. These above results indicated that Ce-MOF@PANI/CC sensor had the practical application potential for determining CBZ. Moreover, the aforementioned results were compared with those obtained from HPLC to further evaluate the accuracy of the Ce-MOF@PANI/CC sensor (Fig. S13). The recovery of the electrochemical experimental detection was basically the same as those of the HPLC with the recovery ranging from 94.23% to 104.62% and the RSDs within 7.32% (Table 2).

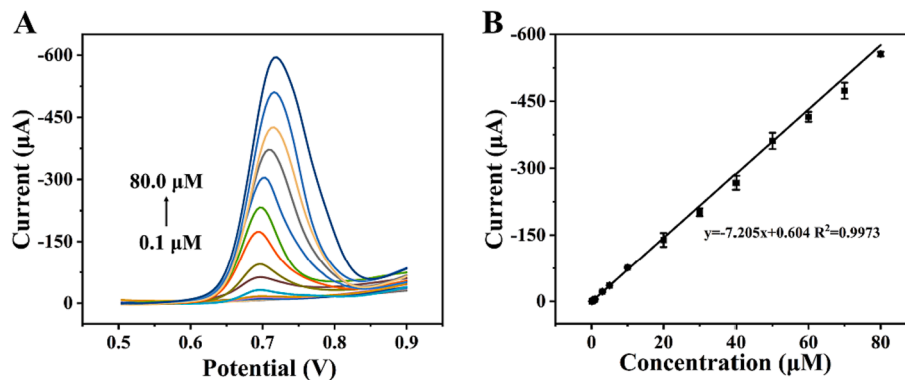


Fig. 4. (A) The curves of DPV in different CBZ concentrations at Ce-MOF@PANI/CC sensor; (B) The linear correlation between different CBZ concentrations and the peak current.

Table 2
Detection of CBZ in real samples (n = 3).

Samples	Added (μM)	This method			HPLC		
		Detection (μM)	Recovery (%)	RSD (%)	Detection (μM)	Recovery (%)	RSD (%)
apple	0	ND	–	–	ND	–	–
	1	0.98 ± 0.04	98.25	4.51	0.98 ± 0.02	97.93	2.10
	5	4.67 ± 0.17	93.44	3.74	4.98 ± 0.11	99.67	2.23
pear	0	ND	–	–	ND	–	–
	1	1.02 ± 0.02	101.61	1.94	1.04 ± 0.04	104.05	4.05
	5	4.81 ± 0.34	96.30	7.15	5.07 ± 0.12	101.34	2.38
tomato	0	ND	–	–	ND	–	–
	1	0.97 ± 0.02	97.05	2.43	1.00 ± 0.01	99.82	1.41
	5	4.94 ± 0.24	98.72	4.80	5.21 ± 0.14	104.20	2.65
cucumber	0	ND	–	–	ND	–	–
	1	0.97 ± 0.04	96.88	4.14	0.99 ± 0.03	99.21	2.91
	5	5.03 ± 0.27	100.59	5.36	4.98 ± 0.22	99.61	4.40
lake	0	ND	–	–	ND	–	–
	1	1.00 ± 0.04	99.59	4.00	1.05 ± 0.04	104.62	3.97
	5	4.69 ± 0.20	93.71	4.31	4.71 ± 0.34	94.23	7.32
tap water	0	ND	–	–	ND	–	–
	1	1.05 ± 0.03	105.47	3.20	1.03 ± 0.03	103.12	3.29
	5	4.62 ± 0.05	92.31	1.08	5.05 ± 0.30	101.03	5.95

ND: Not detected.

4. Conclusion

To summarize, an economy-friendly and simple method was developed to fabricate an electrochemical sensing platform based on Ce-MOF@PANI/CC for sensitive electrochemical determination of CBZ. Ce-MOF could contribute the dispersion of PANI, while PANI further increased conductivity of Ce-MOF. The combination of Ce-MOF and PANI enhanced electrochemical active surface area. Ce-MOF@PANI promoted the absorption of CBZ through pore-size matching effect and π - π stacking and improved catalytic oxidation of CBZ. The developed method exhibited commendable anti-interference, reproducibility, and stability. It had potential for application to determine CBZ in food and environment.

CRedit authorship contribution statement

Rui Zhou: Writing – original draft, Methodology, Investigation, Formal analysis, Conceptualization. **Ling-Zhi Liu:** Methodology, Investigation, Data curation. **Yue-Hong Pang:** Writing – review & editing, Validation, Formal analysis. **Xiao-Fang Shen:** Writing – review & editing, Resources, Project administration, Funding acquisition, Conceptualization.

Declaration of competing interest

The authors declare that they have no known competing financial interests or personal relationships that could have appeared to influence the work reported in this paper.

Data availability

Data will be made available on request.

Acknowledgments

This work was supported by the National Key Research and Development Program of China (2022YFF1100803).

Appendix A. Supplementary data

Supplementary data to this article can be found online at <https://doi.org/10.1016/j.microc.2023.109862>.

References

- [1] S. Chauhan, T. Fatima, A. Dubey, P.S. Chauhan, O. Prakash, P.C. Singh, Integrated application of trichoderma and carbendazim affects the carbendazim extractability and microbial functions in the maize rhizosphere, *J. Soil Sci. Plant Nut.* 23 (2023) 3373–3380, <https://doi.org/10.1007/s42729-023-01254-y>.
- [2] X. Wei, W. Song, Y. Fan, Y. Sun, Z. Li, S. Chen, J. Shi, D. Zhang, X. Zou, X. Xu, A SERS aptasensor based on a flexible substrate for interference-free detection of carbendazim in apple, *Food Chem.* 431 (2024), 137120, <https://doi.org/10.1016/j.foodchem.2023.137120>.
- [3] X. Chen, G. Li, X. Yue, C. Peng, J. Wang, Ratiometric fluorescent detection of carbendazim in foods based on metallic nanoclusters self-assembled nanocomplex, *Food Chem.* 424 (2023), 136478, <https://doi.org/10.1016/j.foodchem.2023.136478>.
- [4] Y.A. Ebedy, M.O. Elshazly, N.H. Hassan, M.A. Ibrahim, E.I. Hassanen, Novel insights into the potential mechanisms underlying carbendazim-induced hepatorenal toxicity in rats, *J. Biochem. Mol. Toxic.* 36 (2022) e23079, <https://doi.org/10.1002/jbt.23079>.
- [5] T. Wang, L. Zhang, J. Zhang, G. Guo, X. Jiang, Z. Zhang, S. Li, Highly sensitive fluorescent quantification of carbendazim by two-dimensional Tb-MOF nanosheets for food safety, *Food Chem.* 416 (2023), 135853, <https://doi.org/10.1016/j.foodchem.2023.135853>.
- [6] Z.A. Abd Elhaleem, Pesticide residues in tomato and tomato products marketed in Majmaah province, KSA, and their impact on human health, *Environ. Sci. Pollut. R* 27 (2020) 8526–8534, <https://doi.org/10.1007/s11356-019-07573-x>.
- [7] Z. Li, J. Nie, Z. Yan, Y. Cheng, F. Lan, Y. Huang, Q. Chen, X. Zhao, A. Li, A monitoring survey and dietary risk assessment for pesticide residues on peaches in China, *Regul. Toxicol. Pharm.* 97 (2018) 152–162, <https://doi.org/10.1016/j.yrtph.2018.06.007>.
- [8] Z. Bao, D. Wang, Y. Zhao, T. Luo, G. Yang, Y. Jin, Insights into enhanced toxic effects by the binary mixture of carbendazim and procymidone on hepatic lipid metabolism in mice, *Sci. Total Environ.* 882 (2023), 163648, <https://doi.org/10.1016/j.scitotenv.2023.163648>.
- [9] X. Chen, W. Li, C. Lu, J. Chu, R. Lin, P. Wang, G. Xie, Q. Gu, D. Wu, B. Chu, Highly sensitive electrochemical detection of carbendazim residues in water by synergistic enhancement of nitrogen-doped carbon nanohorns and polyethyleneimine modified carbon nanotubes, *Sci. Total Environ.* 851 (2022), 158324, <https://doi.org/10.1016/j.scitotenv.2022.158324>.
- [10] K.G. Kim, D.W. Park, G.R. Kang, T.S. Kim, Y. Yang, S.J. Moon, E.A. Choi, D.R. Ha, E.S. Kim, B.S. Cho, Simultaneous determination of plant growth regulator and pesticides in bean sprouts by liquid chromatography–tandem mass spectrometry, *Food Chem.* 208 (2016) 239–244, <https://doi.org/10.1016/j.foodchem.2016.04.002>.
- [11] J. Domínguez Álvarez, M. Mateos Vivas, D. García Gómez, E. Rodríguez-Gonzalo, R. Carabias-Martínez, Capillary electrophoresis coupled to mass spectrometry for the determination of anthelmintic benzimidazoles in eggs using a QuEChERS with preconcentration as sample treatment, *J. Chromatogr. A* 1278 (2013) 166–174, <https://doi.org/10.1016/j.chroma.2012.12.064>.
- [12] H. Liu, Y. Wang, R. Fu, J. Zhou, Y. Liu, Q. Zhao, J. Yao, Y. Cui, C. Wang, B. Jiao, Y. He, A multicolor enzyme-linked immunoassay method for visual readout of carbendazim, *Anal. Methods-UK* 13 (2021) 4256–4265, <https://doi.org/10.1039/D1AY01028J>.
- [13] H. Guo, R. Yang, D. Lei, X. Ma, D. Zhang, P. Li, J. Wang, L. Zhou, W. Kong, Red-emissive carbon dots based fluorescent and smartphone-integrated paper sensors for sensitive detection of carbendazim, *Microchem. J.* 190 (2023), 108586, <https://doi.org/10.1016/j.microc.2023.108586>.

- [14] Q. He, B. Wang, J. Liang, J. Liu, B. Liang, G. Li, Y. Long, G. Zhang, H. Liu, Research on the construction of portable electrochemical sensors for environmental compounds quality monitoring, *Mater. Today Adv.* 17 (2023), 100340, <https://doi.org/10.1016/j.mtdadv.2022.100340>.
- [15] Y. Wu, G. Li, Y. Tian, J. Feng, J. Xiao, J. Liu, X. Liu, Q. He, Electropolymerization of molecularly imprinted polypyrrole film on multiwalled carbon nanotube surface for highly selective and stable determination of carcinogenic amaranth, *J. Electroanal. Chem.* 895 (2021), 115494, <https://doi.org/10.1016/j.jelechem.2021.115494>.
- [16] S. Zhang, P. Ling, Y. Chen, J. Liu, C. Yang, 2D/2D porous $\text{Co}_3\text{O}_4/\text{rGO}$ nanosheets act as an electrochemical sensor for voltammetric tryptophan detection, *Diam. Relat. Mater.* 135 (2023), 109811, <https://doi.org/10.1016/j.diamond.2023.109811>.
- [17] P. Deng, J. Feng, Y. Wei, J. Xiao, J. Li, Q. He, Fast and ultrasensitive trace malachite green detection in aquaculture and fisheries by using hexadecylpyridinium bromide modified electrochemical sensor, *J. Food Compos. Anal.* 102 (2021), 104003, <https://doi.org/10.1016/j.jfca.2021.104003>.
- [18] F. Wang, F. Shi, C. Chen, K. Huang, N. Chen, Z. Xu, Electrochemical fabrication of $\text{Co}(\text{OH})_2$ nanoparticles decorated carbon cloth for non-enzymatic glucose and uric acid detection, *Microchim. Acta* 189 (2022) 385, <https://doi.org/10.1007/s00604-022-05437-9>.
- [19] M. Wasi Ahmad, B. Dey, B. H. Kim, G. Sarkhel, D. J. Yang, S.K. Safdar Hossain, T. Kamal, A. Choudhury, Bimetallic copper-cobalt MOFs anchored carbon nanofibers hybrid mat based electrode for simultaneous determination of dopamine and tyramine, *Microchem. J.* 193 (2023) 109074, <https://doi.org/10.1016/j.microc.2023.109074>.
- [20] S. Singh, A. Numan, Y. Zhan, V. Singh, T. Van Hung, N.D. Nam, A novel highly efficient and ultrasensitive electrochemical detection of toxic mercury (II) ions in canned tuna fish and tap water based on a copper metal-organic framework, *J. Hazard. Mater.* 399 (2020), 123042, <https://doi.org/10.1016/j.jhazmat.2020.123042>.
- [21] E. Mahmoudi, H. Fakhri, A. Hajian, A. Afkhami, H. Bagheri, High-performance electrochemical enzyme sensor for organophosphate pesticide detection using modified metal-organic framework sensing platforms, *Bioelectrochemistry* 130 (2019), 107348, <https://doi.org/10.1016/j.bioelechem.2019.107348>.
- [22] B. Wu, L. Xiao, M. Zhang, C. Yang, Q. Li, G. Li, Q. He, J. Liu, Facile synthesis of dendritic-like CeO_2/rGO composite and application for detection of uric acid and tryptophan simultaneously, *J. Solid State Chem.* 296 (2021), 122023, <https://doi.org/10.1016/j.jssc.2021.122023>.
- [23] P. Deng, J. Feng, J. Xiao, Y. Wei, J. Zuo, J. Li, J. Ding, Q. He, Determination of uric acid in biological fluids by ceria nanoparticles doped reduced graphene oxide nanocomposite voltammetric sensor, *J. Electrochem. Soc.* 168 (2021), 126529, <https://doi.org/10.1149/1945-7111/ac4376>.
- [24] H. Huang, Y. Chen, Z. Chen, J. Chen, Y. Hu, J.J. Zhu, Electrochemical sensor based on Ce-MOF/carbon nanotube composite for the simultaneous discrimination of hydroquinone and catechol, *J. Hazard. Mater.* 416 (2021), 125895, <https://doi.org/10.1016/j.jhazmat.2021.125895>.
- [25] L. Zhang, M. Sun, T. Jing, S. Li, H. Ma, A facile electrochemical sensor based on green synthesis of Cs/Ce-MOF for detection of tryptophan in human serum, *Colloid. Surf. A* 648 (2022), 129225, <https://doi.org/10.1016/j.colsurfa.2022.129225>.
- [26] X. Tu, Y. Xie, X. Ma, F. Gao, L. Gong, D. Wang, L. Lu, G. Liu, Y. Yu, X. Huang, Highly stable reduced graphene oxide-encapsulated Ce-MOF composite as sensing material for electrochemically detecting dichlorophen, *J. Electroanal. Chem.* 848 (2019), 113268, <https://doi.org/10.1016/j.jelechem.2019.113268>.
- [27] S. Wang, Y. Xue, Z. Yu, F. Huang, Y. Jin, Layered 2D MOF nanosheets grown on CNTs substrates for efficient nitrite sensing, *Mater. Today Chem.* 30 (2023), 101490, <https://doi.org/10.1016/j.mtchem.2023.101490>.
- [28] Y. Chen, S. Li, L. Zhang, T. Jing, J. Wang, L. Zhao, F. Li, C. Li, J. Sun, Facile and fast synthesis of three-dimensional Ce-MOF/ $\text{Ti}_3\text{C}_2\text{Tx}$ MXene composite for high performance electrochemical sensing of L-Tryptophan, *J. Solid State Chem.* 308 (2022), 122919, <https://doi.org/10.1016/j.jssc.2022.122919>.
- [29] M.Z. Iqbal, M.M. Faisal, S.R. Ali, S. Farid, A.M. Afzal, Co-MOF/polyaniline-based electrode material for high performance supercapattery devices, *Electrochim. Acta* 346 (2020), 136039, <https://doi.org/10.1016/j.electacta.2020.136039>.
- [30] L. Duy Nguyen, C. Mau Dang, T. Chanh Duc Doan, Highly stable ammonium ion-selective electrodes based on one-pot synthesized gold nanoparticle-reduced graphene oxide as ion-to-electron transducers, *Microchem. J.* 190 (2023) 108717, <https://doi.org/10.1016/j.microc.2023.108717>.
- [31] X. Hou, R. Ding, W. Jiang, Q. Yang, X. Mao, Detection of chlorpyrifos via carbon nanotubes and AuPd nanoparticles-enhanced MXene electrode-based acetylcholinesterase biosensor, *Microchem. J.* 195 (2023), 109319, <https://doi.org/10.1016/j.microc.2023.109319>.
- [32] K. Liu, H. You, G. Jia, Y. Zheng, Y. Huang, Y. Song, M. Yang, L. Zhang, H. Zhang, Hierarchically nanostructured coordination polymer: facile and rapid fabrication and tunable morphologies, *Cryst. Growth Des.* 10 (2010) 790–797, <https://doi.org/10.1021/cg901170j>.
- [33] J. Huang, R.B. Kaner, Nanofiber formation in the chemical polymerization of aniline: a mechanistic study, *Angew. Chem. Int. Edit.* 43 (2004) 5817–5821, <https://doi.org/10.1002/ange.200460616>.
- [34] X. Zhang, F. Hou, H. Li, Y. Yang, Y. Wang, N. Liu, Y. Yang, A strawsheave-like metal organic framework Ce-BTC derivative containing high specific surface area for improving the catalytic activity of CO oxidation reaction, *Micropor. Mesopor. Mat.* 259 (2018) 211–219, <https://doi.org/10.1016/j.micromeso.2017.10.019>.
- [35] J. Zhang, X. Xu, L. Chen, An ultrasensitive electrochemical bisphenol A sensor based on hierarchical Ce-metal-organic framework modified with cetyltrimethylammonium bromide, *Sens. Actu. B-Chem.* 261 (2018) 425–433, <https://doi.org/10.1016/j.snb.2018.01.170>.
- [36] S. Li, Y. Wei, Y. Kong, Y. Tao, C. Yao, R. Zhou, Electrochemical removal of lead ions using paper electrode of polyaniline/attapulgite composites, *Synthetic Met.* 199 (2015) 45–50, <https://doi.org/10.1016/j.synthmet.2014.11.003>.
- [37] Z. Neisi, Z. Ansari Asl, A.S. Dezfuli, Polyaniline/Cu(II) Metal-organic frameworks composite for high performance supercapacitor electrode, *J. Inorg. Organomet. P.* 29 (2019) 1838–1847, <https://doi.org/10.1007/s10904-019-01145-9>.
- [38] N. Sebastian, W. C. Yu, D. Balram, F.S. Al-Mubaddel, M. Tayyab Noman, Functionalization of CNFs surface with β -cyclodextrin and decoration of hematite nanoparticles for detection and degradation of toxic fungicide carbendazim, *Appl. Surf. Sci.* 586 (2022) 152666, <https://doi.org/10.1016/j.apsusc.2022.152666>.
- [39] N. Zhou, Y. Ma, B. Hu, L. He, S. Wang, Z. Zhang, S. Lu, Construction of Ce-MOF@COF hybrid nanostructure: Label-free aptasensor for the ultrasensitive detection of oxytetracycline residues in aqueous solution environments, *Biosens. Bioelectron.* 127 (2019) 92–100, <https://doi.org/10.1016/j.bios.2018.12.024>.
- [40] S. Zhu, A. Xie, X. Tao, J. Zhang, B. Wei, Z. Liu, Y. Tao, S. Luo, Enhanced electrocatalytic performance of CoCu-MOF/polyaniline for glycerol oxidation, *J. Electroanal. Chem.* 857 (2020), 113748, <https://doi.org/10.1016/j.jelechem.2019.113748>.
- [41] T. Kokulnathan, T.J. Wang, F. Ahmed, N. Arshi, Fabrication of flower-like nickel cobalt-layered double hydroxide for electrochemical detection of carbendazim, *Surf. Interfaces* 36 (2023), 102570, <https://doi.org/10.1016/j.surfint.2022.102570>.
- [42] P. Sundaresan, C.C. Fu, S.H. Liu, R.S. Juang, Facile synthesis of chitosan-carbon nanofiber composite supported copper nanoparticles for electrochemical sensing of carbendazim, *Colloid. Surf. A* 625 (2021), 126934, <https://doi.org/10.1016/j.colsurfa.2021.126934>.
- [43] Y. Han, H. Wang, Y. Yu, W. Yang, F. Shang, Z. Li, Impact on ratiometric fluorescence of carbon dots hybridizing with lanthanide in determination of residual Carbendazim in food, *Appl. Surf. Sci.* 606 (2022), 154700, <https://doi.org/10.1016/j.apsusc.2022.154700>.
- [44] R. Cui, D. Xu, X. Xie, Y. Yi, Y. Quan, M. Zhou, J. Gong, Z. Han, G. Zhang, Phosphorus-doped helical carbon nanofibers as enhanced sensing platform for electrochemical detection of carbendazim, *Food Chem.* 221 (2017) 457–463, <https://doi.org/10.1016/j.foodchem.2016.10.094>.
- [45] Y. Xie, F. Gao, X. Tu, X. Ma, R. Dai, G. Peng, Y. Yu, L. Lu, Flake-like neodymium molybdate wrapped with multi-walled carbon nanotubes as an effective electrode material for sensitive electrochemical detection of carbendazim, *J. Electroanal. Chem.* 855 (2019), 113468, <https://doi.org/10.1016/j.jelechem.2019.113468>.
- [46] A. Yamuna, T.W. Chen, S.M. Chen, Synthesis and characterizations of iron antimony oxide nanoparticles and its applications in electrochemical detection of carbendazim in apple juice and paddy water samples, *Food Chem.* 373 (2022), 131569, <https://doi.org/10.1016/j.foodchem.2021.131569>.
- [47] Y. Yao, Y. Wen, L. Zhang, Z. Wang, H. Zhang, J. Xu, Electrochemical recognition and trace-level detection of bactericide carbendazim using carboxylic group functionalized poly(3,4-ethylenedioxythiophene) mimic electrode, *Anal. Chim. Acta* 831 (2014) 38–49, <https://doi.org/10.1016/j.aca.2014.04.059>.
- [48] A. Yamuna, T.W. Chen, S.M. Chen, T.Y. Jiang, Facile synthesis of single-crystalline Fe-doped copper vanadate nanoparticles for the voltammetric monitoring of lethal hazardous fungicide carbendazim, *Microchim. Acta* 188 (2021) 277, <https://doi.org/10.1007/s00604-021-04941-8>.
- [49] H. Zhao, B. Liu, Y. Li, B. Li, H. Ma, S. Komarneni, One-pot green hydrothermal synthesis of bio-derived nitrogen-doped carbon sheets embedded with zirconia nanoparticles for electrochemical sensing of methyl parathion, *Ceram. Int.* 46 (2020) 19713–19722, <https://doi.org/10.1016/j.ceramint.2020.04.277>.
- [50] C. Tian, S. Zhang, H. Wang, C. Chen, Z. Han, M. Chen, Y. Zhu, R. Cui, G. Zhang, Three-dimensional nanoporous copper and reduced graphene oxide composites as enhanced sensing platform for electrochemical detection of carbendazim, *J. Electroanal. Chem.* 847 (2019), 113243, <https://doi.org/10.1016/j.jelechem.2019.113243>.
- [51] Y. Zhou, Y. Li, P. Han, Y. Dang, M. Zhu, Q. Li, Y. Fu, A novel low-dimensional heteroatom doped Nd_2O_3 nanostructure for enhanced electrochemical sensing of carbendazim, *New J. Chem.* 43 (2019) 14009–14019, <https://doi.org/10.1039/C9NJ02778E>.
- [52] R. Liu, Y. Chang, F. Li, V. Dubovyk, D. Li, Q. Ran, H. Zhao, Highly sensitive detection of carbendazim in juices based on mung bean-derived porous carbon@chitosan composite modified electrochemical sensor, *Food Chem.* 392 (2022), 133301, <https://doi.org/10.1016/j.foodchem.2022.133301>.
- [53] C.A. Razzino, L.F. Sgobbi, T.C. Canevari, J. Cancino, S.A.S. Machado, Sensitive determination of carbendazim in orange juice by electrode modified with hybrid material, *Food Chem.* 170 (2015) 360–365, <https://doi.org/10.1016/j.foodchem.2014.08.085>.
- [54] W.F. Ribeiro, T.M.G. Selva, I.C. Lopes, E.C.S. Coelho, S.G. Lemos, F. Caxico de Abreu, V. Bernardo do Nascimento, M.C. Ugulino de Araújo, Electroanalytical determination of carbendazim by square wave adsorptive stripping voltammetry with a multiwalled carbon nanotubes modified electrode, *Anal. Methods-UK* 3 (2011) 1202–1206, <https://doi.org/10.1039/C0AY00723D>.
- [55] G.A. Fozing Mekeuo, C. Despas, C. Pégyu Nansu Njiki, A. Walcarius, E. Ngameni, Preparation of functionalized ayous sawdust-carbon nanotubes composite for the electrochemical determination of carbendazim pesticide, *Electroanalysis* 34 (2022) 667–676, <https://doi.org/10.1002/elan.202100262>.